MCT4 blockade increases the efficacy of immune checkpoint blockade

Nathalie Babl [iD],[1] Sonja-Maria Decking,[1,2,3] Florian Voll,[1,3] Michael Althammer,[1] Ada Sala-Hojman,[4] Roberta Ferretti,[5] Clarissa Korf,[2] Christian Schmidl,[3] Lisa Schmidleithner,[3] Benedikt Nerb,[3] Carina Matos,[1] Gudrun E Koehl,[6] Peter Siska [iD],[1] Christina Bruss,[1,7] Fabian Kellermeier,[8] Katja Dettmer,[8] Peter J Oefner,[8] Marvin Wichland,[2] Ines Ugele,[2] Christopher Bohr,[2] Wolfgang Herr,[1] Shivapriya Ramaswamy,[5] Timo Heinrich,[4] Christian Herhaus,[4] Marina Kreutz,[1,3] Kathrin Renner[1,2]

ABSTRACT

Background & Aims Intratumoral lactate accumulation and acidosis impair T-cell function and antitumor immunity. Interestingly, expression of the lactate transporter monocarboxylate transporter (MCT) 4, but not MCT1, turned out to be prognostic for the survival of patients with rectal cancer, indicating that single MCT4 blockade might be a promising strategy to overcome glycolysis-related therapy resistance.

Methods To determine whether blockade of MCT4 alone is sufficient to improve the efficacy of immune checkpoint blockade (ICB) therapy, we examined the effects of the selective MCT1 inhibitor AZD3965 and a novel MCT4 inhibitor in a colorectal carcinoma (CRC) tumor spheroid model co-cultured with blood leukocytes in vitro and the MC38 murine CRC model in vivo in combination with an antibody against programmed cell death ligand-1(PD-L1).

Results Inhibition of MCT4 was sufficient to reduce lactate efflux in three-dimensional (3D) CRC spheroids but not in two-dimensional cell-cultures. Co-administration of the MCT4 inhibitor and ICB augmented immune cell infiltration, T-cell function and decreased CRC spheroid viability in a 3D co-culture model of human CRC spheroids with blood leukocytes. Accordingly, combination of MCT4 and ICB increased intratumoral pH, improved leukocyte infiltration and T-cell activation, delayed tumor growth, and prolonged survival in vivo. MCT1 inhibition exerted no further beneficial impact.

Conclusions These findings demonstrate that single MCT4 inhibition represents a novel therapeutic approach to reverse lactic-acid driven immunosuppression and might be suitable to improve ICB efficacy.

WHAT IS ALREADY KNOWN ON THIS TOPIC

⇒ Lactic acidosis of Warburg tumors is associated with immune checkpoint blockade (ICB) resistance.
⇒ Targeting both lactate transporters, the ubiquitously-expressed monocarboxylate transporter (MCT)1 and the glycolysis-related MCT4, augments ICB.

WHAT THIS STUDY ADDS

⇒ MCT4, but not MCT1, is prognostic for survival of rectal cancer.
⇒ Single MCT4 inhibition, using a novel small molecule inhibitor, was sufficient to support T-cell function, and in combination with ICB increased immune cell infiltration resulting in decreased colorectal carcinoma (CRC) spheroid viability in a three-dimensional co-culture model of human CRC spheroids with blood leukocytes.
⇒ In contrast, specific and complete blockade of MCT1 and MCT4 could not further augment ICB efficacy.
⇒ Combination of single MCT4 inhibitor and ICB increased intratumoral pH, improved leukocyte infiltration and T-cell activation, delayed tumor growth, and prolonged survival in an in vivo MC38 mouse model.

HOW THIS STUDY MIGHT AFFECT RESEARCH, PRACTICE OR POLICY

⇒ Blocking the glycolysis-related MCT4 might be sufficient to overcome glycolysis-related therapy resistance and exert less severe side effects.

BACKGROUND

Alterations in the energy metabolism of tumor cells are a hallmark of cancer.[1] Accelerated glucose metabolism and a highly elevated turn-over of pyruvate into lactate even in the presence of oxygen, the so-called Warburg phenotype, is a well-known metabolic feature of different tumor entities and linked to limited therapeutic response and poor patient prognosis.[2][3] Moreover, the Warburg phenotype represents a metabolic checkpoint contributing to immune evasion and poor response to immunotherapy. To maintain glycolytic flux, the generated lactate needs to be efficiently secreted by proton-coupled monocarboxylate transporters (MCT) 1 and 4. Lactate transport via MCTs results in lactate accumulation and concomitant acidification in the tumor microenvironment, fostering immunosuppressive cell populations and limiting antitumor immune

effector cells.[4 5] Under these conditions, tumor-associated macrophages exhibit tumor-promoting features such as increased secretion of interleukin 6 (IL-6), transforming growth factor β, and vascular endothelial growth factor.[6 7] Moreover, regulatory T cell (Treg) function is preserved, whereas T and natural killer (NK) cell-mediated antitumor immunity is severely hampered.[8–11] The number of infiltrating effector T cells is reduced as well as the expression of important mediators of antitumor immunity such as interferon γ (IFNγ). Vice versa, reducing lactate secretion by lowering the expression of lactate dehydrogenase (LDH) in tumor cells improves T and NK cell infiltration and function, and tumor growth control.[9] Accordingly, the administration of an LDH inhibitor increased the efficacy of adoptive T-cell transfer in a melanoma model[12] and an LDH knock-out improved the response to immune checkpoint blockade (ICB).[13]

The recognition of increased glucose metabolism in cancer as a potential therapeutic target has spurred the development of inhibitors of glucose transporters[14] and LDH.[15] Further, AZD3965, an inhibitor specific for MCT1 was reported in 2008 by Murray et al,[16] and it has been tested clinically (NCT01791595). MCT1 is almost ubiquitously expressed, whereas MCT4 is mainly found on highly glycolytic cells. Expression of MCT4 and its chaperone CD147 is predictive for overall survival (OS) in different tumor entities including head and neck cancer, breast cancer, hepatocellular cancer and pancreatic cancer.[17–20] Increased expression of MCT1, MCT4 and CD147 as well as the glucose transporter GLUT1 is detected in colorectal cancer (CRC) tissue,[21 22] the third most common cancer in Western countries.[23] It correlates with lymph node and distant metastasis[24] and poor survival.[25 26] The PI3K/AKT/mTOR signaling pathway is frequently activated and fosters, via hypoxia-inducible factor 1α (HIF-1α), a metabolic rewiring towards glycolysis in CRC.[27] Accordingly, increased lactate levels were detected in CRC tumor samples compared with adjacent mucosa,[28] with the rectal cancer subgroup showing the highest lactate concentrations.[29]

In addition to the prognostic relevance of glucose metabolism-related proteins and signatures,[30] infiltration of CD3^{+} T cells in general and cytotoxic CD8^{+} T cells, in particular, in the tumor core and at the invasive margins is highly predictive for OS in patients with CRC[31–33] and used for CRC classification in addition to classical tumor-node-metastasis (TNM) staging.[34] Current strategies for treatment of CRC are limited and ICB therapy is restricted to a small subset (15%) of tumors with mismatch repair deficiency (MMRd)/microsatellite instability (MSI).[35] MSI CRC tumors exhibit higher numbers of immune cells, particularly CD8^{+} tumor-infiltrating T cells (TILs) and T helper 1 CD4^{+} cells,[36] which could contribute to a better response to ICB. As increased glycolysis negatively correlates with T cell counts and contributes to ICB resistance,[2 37] co-administration of anti-glycolytic drugs might increase ICB efficacy. In our previous study, we showed that the non-steroidal anti-inflammatory drug diclofenac,

which blocks both MCT1 and MCT4 with a 10-fold higher Ki for MCT4, supports blockade of programmed cell death protein-1 (PD-1) and cytotoxic T-lymphocyte-associated protein-4 (CTLA-4) in vitro and in vivo.[13]

In this study, we aimed to delineate whether blockade of MCT4 alone is sufficient to enhance efficacy of ICB therapy or whether it needed to be combined with MCT1 blockade. Therefore, we assessed the impact of the selective MCT1 inhibitor (MCT1i) AZD3965 and a novel MCT4 inhibitor (MCT4i)[38] on tumor growth in a CRC model in combination with anti-programmed cell death ligand-1(PD-L1) antibodies. Our results, together with the results of a recently published study on hepatocellular carcinoma,[17] demonstrate that selective MCT4 inhibition is sufficient to improve the response to ICB in MCT4-driven tumors by reducing tumor-derived lactic acidosis. Finally, as the in vitro results obtained with a human co-culture model of tumor spheroids and blood leukocytes were comparable to our in vivo results, the former might help to refine animal experiments.

RESULTS

MCT4 expression correlates with survival of patients with rectal cancer and its blockade lowers secretion of immunosuppressive lactic acid in a tumor spheroid model

We first evaluated whether MCT1 or MCT4 expression was associated with the survival of patients with CRC by analyzing The Cancer Genome Atlas (TCGA) data. While MCT1 expression correlated with survival neither in the combined nor in the separate analysis of patients with colon and rectal cancer, MCT4 expression turned out to be prognostic for survival of patients with rectal cancer (figure 1A). The negative impact of MCT4 expression on the prognosis of patients with rectal cancer was confirmed in a second cohort (online supplemental figure S1A). In the same cohort, we detected a negative correlation between MCT4 and CD8 expression, suggesting less T-cell infiltration and a worse antitumor immunity in MCT4-expressing tumors (online supplemental figure S1A).

Next, we aimed to investigate whether the administration of specific MCT inhibitors could mitigate the Warburg phenotype of colon carcinoma cells. As a model system, we chose the human colon carcinoma cell line HCT116 and analyzed the MCT expression profile. In two-dimensional (2D) cultures, both transporters (figure 1B and online supplemental figure S1B) as well as CD147, the chaperon required for their membrane localization (figure 1C), were expressed. Accordingly, we observed a continuous acidification of the culture medium over time (online supplemental figure S1C) and concomitant lactate secretion (figure 1D), reflecting the Warburg phenotype. To reduce lactic acid secretion, we administered specific inhibitors for MCT1/2 (MCT1i, AZD3965, displaying a 6-fold higher selective binding activity for MCT1 over MCT2) and MCT4 (MSC-4381) and combinations thereof. Both drugs show a high specificity for their targets and display half maximal inhibitory concentration
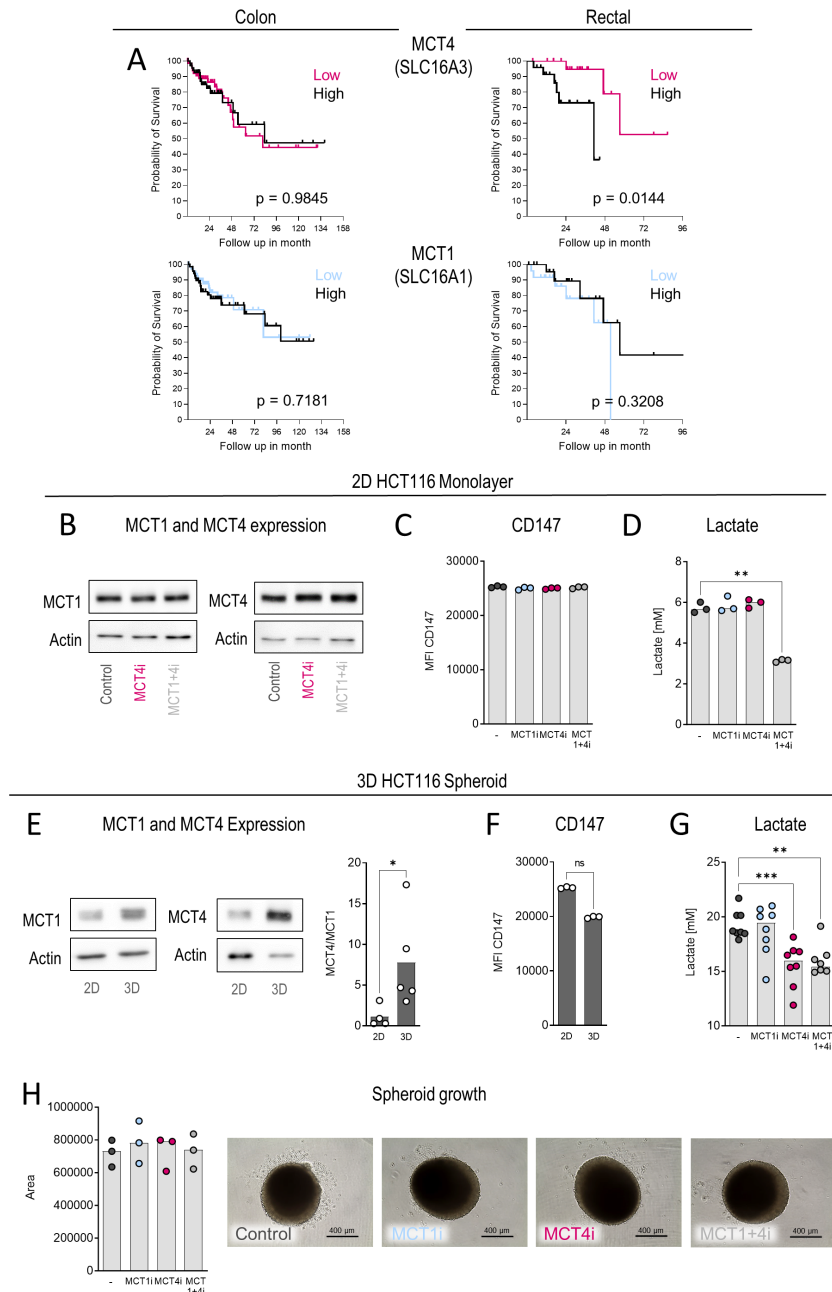
Figure 1 MCT4 expression negatively correlates with overall survival in rectal cancer and its inhibition reduces lactic acid secretion. (A) Transcriptome data from 326 colon cancer and 186 rectal cancer samples were obtained from The Cancer Genome Atlas database using the UCSC Xena platform: Expression is depicted as log2(fpkm-uq+1) values. Log-rank (Mantel-Cox) test was used to calculate differences in overall survival when comparing the upper and the lower quartile of samples. (B–D) 2D cultures of HCT116 cells were treated with 0.1 µM MCT1 inhibitor (MCT1i) and/or MCT4 inhibitor (MCT4i). (B) Protein expression of MCT1 and MCT4 was analyzed by Western blot analysis after 24 hours of treatment. One representative blot out of three independent experiments is shown. (C) CD147 expression was determined by flow cytometry after 24 hours of treatment. MFI, median fluorescence intensity. (D) Lactate concentrations were measured after 24 hours in culture supernatants. (E–H) HCT116 were cultured either as monolayer (2D) or spheroids (3D). HCT116 monolayers were treated for 24 hours and spheroids for 9 days with 0.1 µM MCT1i and MCT4i. (E) MCT expression was analyzed in whole-cell lysates of HCT116 monolayers or HCT116 spheroids by Western blot analysis (n=5). Ratio of MCT4/MCT1 expression was quantified by Image J. (F) CD147 expression was determined by flow cytometry. (G) Lactate concentrations were measured after 9 days in 3D HCT116 spheroid culture supernatants. (H) Morphology of treated spheroids was assessed after 9 days of treatment and images were recorded using the EVOS system (n=8). One representative picture out of eight independent experiments is shown. Area was quantified in three experiments using ImageJ. Median values and single data points are shown. (B–H) Depicted are representative blots or median values with single data points. Significance was determined using Mann-Whitney U test for comparison of two groups and one-way ANOVA and post hoc Bonferroni multiple comparison test when comparing more than two groups (*p<0.05; **p<0.01; ***p<0.001), unless indicated otherwise. ANOVA, analysis of variance; MCT, monocarboxylate transporter; 2D, two-dimensional; 3D, three-dimensional.

(IC_{50}) values in the low nM range,[38 39] therefore we applied 100 nM each. In line with published data,[13 40 41] administration of either AZD3965 or MSC-4381 had no effect on lactate secretion in 2D cultures, whereas the combined treatment resulted in an approximately 50% reduction (figure 1D) along with an increase in pH (online supplemental figure S1C). Treatments did not lower protein expression of the transporters and CD147, thus the decrease in extracellular lactate can be delineated to a blockade of the transporter activity (figure 1B,C and online supplemental figure S1B). The co-administration of both MCT inhibitors significantly decreased proliferation (online supplemental figure S1D), but it did not impact cell viability (online supplemental figure S1E).

We confirmed these results by applying a second MCT4i (AZD0095, AZD4i)[42] and obtained comparable data (online supplemental figure S1F). However, a higher concentration of AZD4i was necessary to obtain similar effects on proliferation compared with 100 nM of MSC-4381 (online supplemental figure S1D,F). Viability was not affected even with higher doses (online supplemental figure S1F). Based on these results, the MSC-4381 compound was used to block MCT4 throughout the whole study.

As 2D-monolayer cultures hardly reflect the metabolic situation in a three-dimensional (3D) tumor, we generated tumor spheroids. The 3D-spheroids reflect the metabolic tumor setting with regard to nutrient gradients, oxygen limitation and the local accumulation of secreted metabolites.[43] Tidwell *et al* recently compared the metabolism of 2D and 3D cultured HCT116 and found increased glycolytic activity and MCT4 expression in tumor spheroids compared with monolayer cultures.[44] Likewise, we observed an upregulation of MCTs in 3D HCT116 spheroids with a stronger effect on MCT4, increasing the MCT4/MCT1 ratio (figure 1E), whereas the expression of CD147 was hardly affected (figure 1F). Consistently, MCT4 blockade significantly decreased lactate secretion, while co-application of MCT1i had no further impact (figure 1G). Nevertheless, both MCT inhibitors did not impact spheroid growth, even when administered in combination (figure 1H).

T-cell function is not affected by selective MCT blockade

As previously published, T-cell infiltration and function are important determinants of survival in patients with CRC.[31 32] To ensure that MCT inhibition had no adverse effects, the functionality of freshly stimulated bulk T cells (CD3$^+$) as well as CD8$^+$ cytotoxic T cells isolated from mononuclear cells (MNCs) from healthy donors was investigated. MCT1 and MCT4 are expressed in human T-cell populations beyond 48 hours of activation (figure 2A and online supplemental figure S2A), along with CD147 (figure 2B and online supplemental figure S2B). Neither single nor combined MCT inhibitor administration affected CD3 or CD8 T-cell viability (figure 2C and online supplemental figure S2C). Interestingly, MCT1/2 but not MCT4 inhibition alone reduced

lactate secretion and concomitantly glucose uptake, which was even more pronounced by combined MCT blockade (figure 2D and online supplemental figure S2D). To gain further insight in metabolic alterations in the presence of MCT inhibitors we investigated cellular oxygen consumption under cell culture conditions over time. In bulk CD3$^+$ T cells and CD8$^+$ T cells respiration was preserved in the presence of MCT4i, however, MCT1i reduced cellular oxygen consumption and the combined treatment exerted a further reduction (figure 2E and online supplemental figure S2E). Furthermore, while the dual treatment resulted in lowered CD147 expression, a consistent modulation of MCT expression was not observed (figure 2A, online supplemental figure S2A). The strong metabolic effect of combined MCT inhibition translated into a reduced proliferation (figure 2F and online supplemental figure S2F).

As T-cell effector functions are important mediators of antitumor immunity, the impact of MCT blockade on activation related surface markers and cytokine production was examined. The stimulation-induced increase in CD25, CD137 and CD69 expression was preserved in the presence of MCT inhibitors in bulk CD3$^+$ as well as in purified CD8$^+$ T cells (figure 2G and online supplemental figure S2G). Importantly, the secretion of the effector cytokines IFNγ and tumor necrosis factor (TNF) was maintained even after blocking MCT1/2/4 simultaneously (figure 2H and online supplemental figure S2H) indicating that reduced respiration still allows effector functions but limits proliferation. Thus, dual MCT inhibition reduced cellular respiration, regarded as important in the tumor microenvironment, and diminished proliferation without affecting effector functions in CD3+ T cells and CD8+ T cells.

Single MCT4 inhibition supports T-cell function and fosters ICB in a 3D co-culture model of HCT116 with peripheral blood leukocytes

Next, we aimed to elucidate whether MCT blockade supported T-cell function and response to ICB in a 3D co-culture model of HCT116 spheroids and whole blood leukocytes isolated from blood of healthy donors. HCT116 cells express comparable high levels of the immune checkpoint PD-L1 in 2D and 3D culture (online supplemental figure S3A), probably rendering them sensitive to T-cell-mediated killing in the presence of anti-PD-L1 antibodies. However, as HCT116 cells are highly glycolytic, combined ICB and MCT blockade, reducing the secretion of immunosuppressive lactic acid, might be superior to ICB alone. To test this hypothesis, we established a 3D co-culture model of HCT116 tumor spheroids with human peripheral immune cells (figure 3A). HCT116 spheroids were grown for 3 days, and subsequently incubated for further 9 days in the presence or absence of MCT inhibitors. Thereafter, lactate levels were determined in culture media and co-culture with immune cells was initiated. To better mimic the physiological environment, whole blood leukocytes, including granulocytes, were added to spheroid
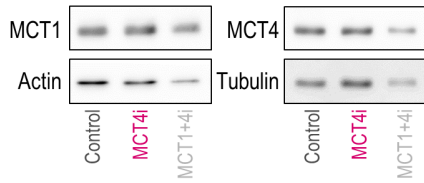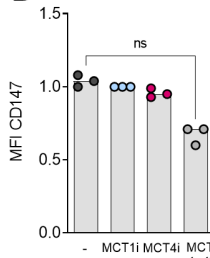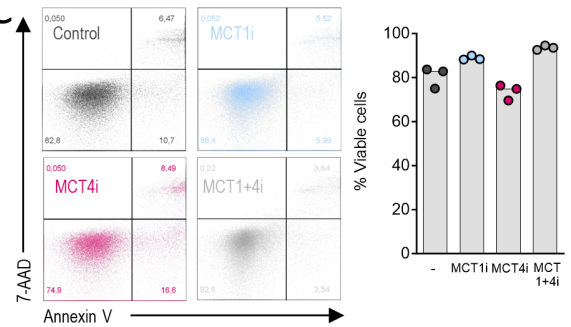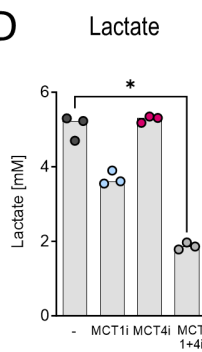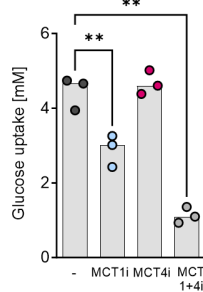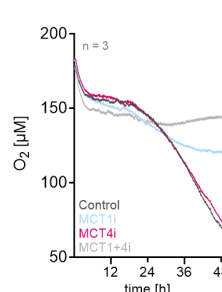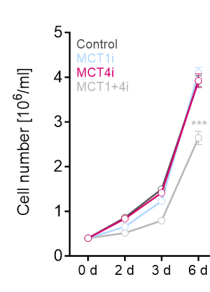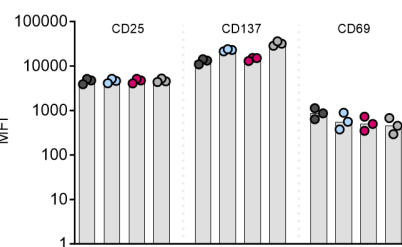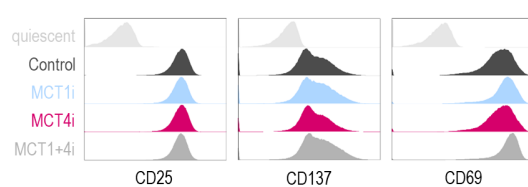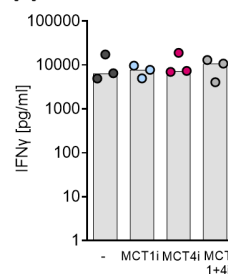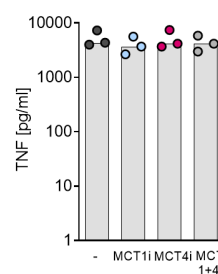
Figure 2 CD3^{+} T-cell function on MCT inhibition. CD3^{+} T cells were isolated from MNCs of healthy donors, stimulated with αCD3/CD28 Dynabeads at a cell-to-bead ratio of 1:1 in the presence of 25 IU/mL IL-2 and treated with 0.1 μM each, either MCT1 inhibitor (MCT1i) and/or MCT4 inhibitor (MCT4i). (A) Protein expression of MCT1 and MCT4 was analyzed in whole-cell lysates by Western blot analysis after 48 hours of stimulation/treatment (n=5). (B) CD147 expression was determined by flow cytometry after 48 hours of treatment. MFI, median fluorescence intensity. (C) Viability was assessed after 72 hours of treatment by Annexin V/7-AAD staining followed by flow cytometric analysis. Viable cells were designated as Annexin V/ 7-AAD double negative. (D) Lactate and glucose concentrations were measured after 48 hours of treatment in culture supernatants. (E) Oxygen consumption was monitored by the PreSens technology. (F) Cell number was analyzed after 72 hours of treatment using the CASY system. Depicted are mean values with SEM. (G) CD25, CD137, and CD69 expression were determined by flow cytometry after 48 hours of treatment. (H) Cytokine levels in culture supernatants were measured by ELISA. (A–H) Depicted are representative blots or summarized values as median values with single data points, unless indicated otherwise. Significance was determined using one-way ANOVA and post hoc Bonferroni multiple comparison test, except for (G) (*p<0.05; **p<0.01). ANOVA, analysis of variance; CASY, cell counter and analyzer system; IFNγ, interferon γ; IL, interleukin; MCT, monocarboxylate transporter; MNCs, mononuclear cells; TNF, tumor necrosis factor.
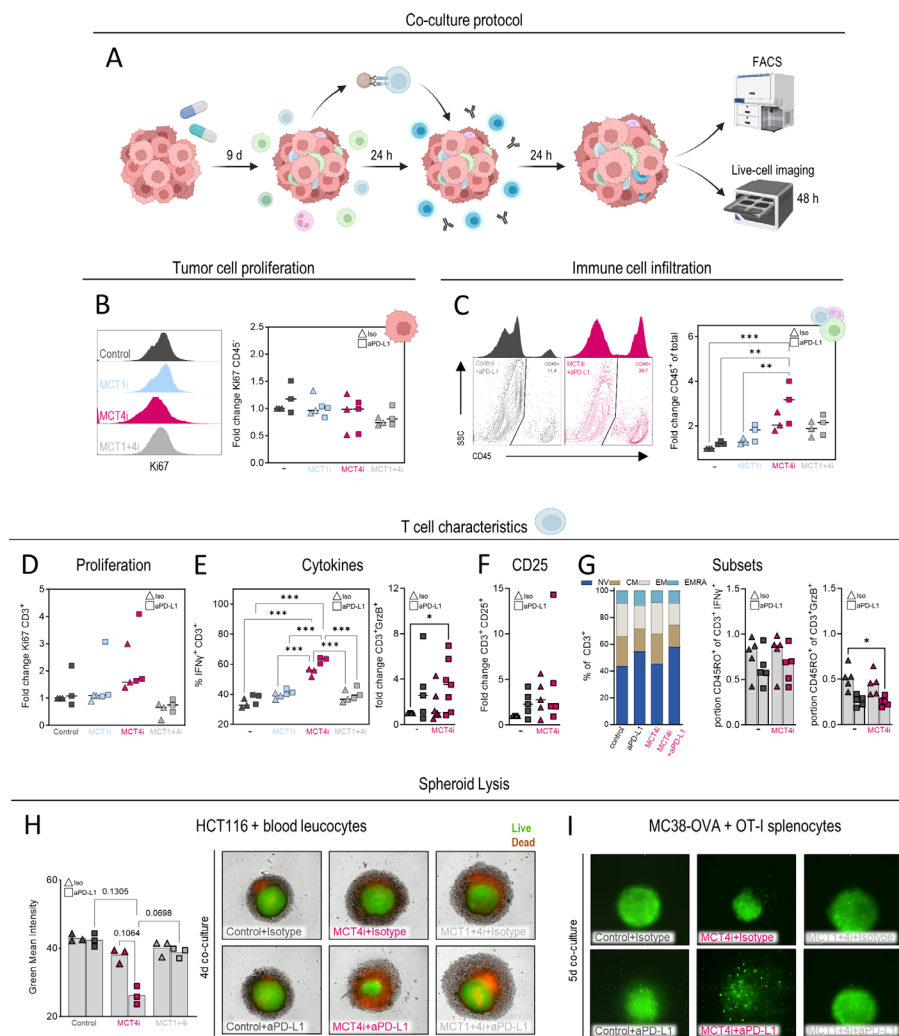
Figure 3 Selective MCT4 inhibition supports T-cell function and potentiates ICB in a 3D co-culture model of HCT116 spheroids with immune cells. (A) Co-culture protocol: HCT116 spheroids were treated with inhibitors for 9 days. Whole blood leucocytes were added to HCT116 spheroids for 24 hours. In parallel, T cells were stimulated for 24 hours with αCD3/CD28 Dynabeads and added the next day together with human aPD-L1 antibody or the respective isotype control (Iso) for additional 24 hours (final concentration 10 µg/mL, respectively). Spheroids were harvested and prepared either for subsequent flow cytometry analysis or for live-cell imaging. Created with BioRender.com. (B–F) Single cell suspensions were prepared from spheroids. (B) Tumor cell proliferation was determined by Ki67 staining and analyzed by flow cytometry in viable CD45− cells. (C) Fold change of viable CD45+ infiltrated immune cells after 48 hours co-culture. (D–F) Gated on viable cells. (D) T-cell proliferation was determined by Ki67 staining and analysis by flow cytometry after 48 hours of co-culture. (E) Percentage of Interferon γ (IFNγ+) or fold change in granzyme B (GrzB+) positive T cells among CD45+ leukocytes after 48 hours of co-culture are shown. (F) Fold change of CD25 expressing CD3+T cells among CD45+ leukocytes is determined by flow cytometry after 48 hours of co-culture. (G) T-cell subset distribution (NV, EM, CM, EMRA) and portion of cytokine expression in memory (CD45RO+) T cells was investigated according to CD45RO and CCR7 surface staining after 48 hours of co-culture (see gating strategy in online supplemental figure S3B). (H) After 48 hours of co-culture, spheroids were washed, fresh medium containing respective treatments and Cyto3D Live-Dead Assay Kit was added and spheroids with infiltrated immune cells were monitored under cell culture conditions for 48 hours using the Incucyte Live Cell Imaging System. Representative pictures of three independent experiments after 4 days of co-culture with immune cells. Green fluorescence=viable cells (Acridine Orange+), red=dead cells (Propidium Iodide+). Mean green fluorescence intensity was quantified as a measure of cell viability. (I) MC38-OVA-GFP spheroids, treated with or without MCTi, were co-cultured with B-cell depleted unstimulated OT-I splenocytes and 24 hours pre-activated splenocytes along with aPD-L1 and respective isotype (final concentration 10 µg/mL). 48 hours later, spheroids were harvested, treatments refreshed and spheroid viability monitored by means of GFP fluorescence (green) using the Incucyte Live Cell Imaging System. Representative pictures of one of two independent experiments after 5 days of co-culture with immune cells are shown. (B–I) Depicted are representative blots or pictures and summarized values as median values with single data points, unless indicated otherwise. Significance was determined using one-way ANOVA and post hoc Bonferroni multiple comparison test (*p<0.05; **p<0.01; ***p<0.001; digits indicate exact p values). ANOVA, analysis of variance; aPD-L1, anti-programmed cell death ligand-1; CM, central memory; EM, effector memory; EMRA, effector memory CD45RA re-expressing; FACS, fluorescence activated cell sorting; ICB, immune checkpoint blockade; MCT, monocarboxylate transporter; MCTi, MCT inhibitor; NV, naïve; 3D, three-dimensional.

cultures. Furthermore, a portion of T cells from the same donor was pre-stimulated for 24 hours and added to the co-culture, reflecting the invasion of T cells activated in the lymph node. After a total of 48 hours, spheroids were picked and non-infiltrated immune cells carefully washed away, single cell suspensions were generated and analyzed by flow cytometry (see gating strategy in online supplemental figure S3B). Proliferation (figure 3B) and viability (data not shown) were not affected by either treatment. However, MCT4 inhibition in combination with human anti-PD-L1 antibody resulted in a significant increase in leukocyte (CD45$^+$ cells) abundance (figure 3C). Neither ICB nor MCT1i alone elevated CD45$^+$ cell infiltration, while MCT4i alone led to a mild increase. Notably, double MCT blockade combined with ICB diminished the positive effect of dual MCT4i and anti-PD-L1 treatment (figure 3C). MCT1i prevented the MCT4i effect, although dual MCT blockade did reduce lactate (figure 1G). Proliferation on triple combination was even reduced (figure 3D). This might be related to the observed metabolic impairment of T cells, such as the decrease in respiration, glucose metabolism and proliferation (figure 2D–F) on dual MCTi treatment, and it is in line with the reported importance of metabolic activity for T-cell function in tumors.[45]

The elevated leukocyte levels could not be linked to a specific impact on a single immune cell population as immune cell composition in terms of T cell (CD3$^+$), Treg (CD4$^+$FOXP3^{++}), monocyte (CD14$^+$) and granulocyte (CD66b$^+$) frequency was not altered (data not shown), and T-cell proliferation was not significantly increased (figure 3D). However, the percentage of IFNγ positive T cells was significantly upregulated by MCT4i, while neither MCT1i nor ICB exerted a significant effect (figure 3E, online supplemental table S1).

Antitumor activity of T cells requires synthesis of perforin and granzymes that synergize to mediate apoptosis of target cells. Further exploring T-cell characteristics on MCT4i and ICB treatment, we detected an increase in granzyme B (GrzB) and perforin expressing T cells (figure 3E and online supplemental figure S3C). Whereas the elevation in perforin was related to MCT4i, the combined treatment with aPD-L1 resulted in a significant increase in GrzB (figure 3E). By trend increased numbers of CD25 (figure 3F), CD137 and PD-1 expressing T cells further reflect improved T-cell activation (online supplemental figure S3D). Treatment related shifts in the CD4$^+$ to CD8$^+$ T cell ratio (data not shown) or in percentage of naïve (NV), central memory (CM), effector memory (EM) and effector memory CD45RA re-expressing (EMRA) CD3 T cells were not observed (figure 3G). However, single aPD-L1 treatment or combination with MCT4i reduced the portion of CD45RO$^+$ cytokine expressing T cells (figure 3G and online supplemental figure S3E), indicating a more NV phenotype on aPD-L1 treatment, probably due to suppressed PD-1 signaling. More than 90% of IFNγ+ memory T cells co-expressed CCR7 treatment independent, thus belong to the CM subset (data not shown).

T-cell function is highly sensitive to lactic acid, therefore, we aimed to revert the effect of MCT4i by exogenous administration of lactic acid or hydrochloric acid (HCl) on day 12 to reach same pH levels as in the control condition before the addition of immune cells. However, short-term administration of lactic acid or HCl to spheroid cultures, could not reverse the positive effect of MCT4i on IFNγ (online supplemental figure S3F) or GrzB (data not shown) indicating that short-term exogenous manipulation of spheroid cultures may not fully translate into changes inside compact 3D tumor spheroids. Thus, we replaced MCT4i administration on day 3 with bicarbonate to increase the buffering capacity of our culture medium. Long-term buffering in combination with aPD-L1 significantly increased, according to MCT4i, the portion of CD45$^+$ leukocytes. Moreover, an elevated percentage of T cells among leukocytes was detected (online supplemental figure S3G). However, cytokine expression in T cells was not significantly increased (data not shown), suggesting that not only changes in the pH are responsible for the improvement in the cytokine response.

In accordance with the higher number of infiltrated cytokine expressing T cells in the presence of MCT4i, a prolonged treatment with MCT4i and aPD-L1 antibody reduced spheroid viability (figure 3H). Notably, this effect was mediated by infiltrated immune cells, as all cells remaining outside the spheroid were washed away after 48 hours. Interestingly, spheroid lysis was not affected by CD8 depletion (online supplemental figure S3H). Finally, we investigated whether MCT4i administration potentiates an antigen specific response in a co-culture model of ovalbumin (OVA) expressing MC38 spheroids and splenocytes from OT-I mice. The combined treatment of MCT4i and aPD-L1 strongly fostered spheroid lysis (figure 3I).

To prove the specificity of the effects observed in response to MCT4i, we knocked-out the respective transporter in HCT116 cells. Knock-out efficacy was confirmed by western blot in cells grown either in 2D or 3D (online supplemental figure S3I), and CD147 expression was only marginally affected (online supplemental figure S3J). As previously shown, single MCT4 knock-out did not alter lactate secretion compared with wildtype cells[40 41] (figure 1G, online supplemental figure S3K). However, it rendered tumor cells sensitive to MCT1 blockade and, as expected, resistant to MCT4 inhibition (online supplemental figure S3K). As for HCT116^{wt} tumor cells, proliferation was not affected by either treatment (online supplemental figure S3L). In line with the impact on lactate secretion, MCT1i increased the number of infiltrating CD45$^+$ leukocytes (online supplemental figure S3M). The frequency of T cells, Tregs, monocytes or granulocytes was not affected by either treatment (data not shown). T-cell proliferation was not substantially affected (online supplemental figure S3N), but IFNγ expression was significantly elevated in the presence of aPD-L1 antibody and MCT inhibition, as expected more pronounced by MCT1i (online supplemental figure S3O). However,

there was still an effect of the MCT4i, indicating a tumor independent impact. Similar to HCT116[wt] spheroids, administration of both MCT inhibitors exerted no positive impact on CD45^{+} leukocyte infiltration or IFNγ expression (online supplemental figure S3M,O).

To sum up, the combination of MCT4i and ICB increased the number of infiltrating leukocytes, IFNγ, granzyme B and perforin expressing T cells and resulted in the lysis of HCT116[wt] tumor spheroids. Moreover, the combinatorial treatment potentiates an antigen specific response.

MCT4 blockade improves the efficacy of immune checkpoint blockade in vivo

Based on our results obtained in the human CRC spheroid co-culture model, we translated our findings to the murine colon carcinoma MC38 3D spheroids co-cultured with splenocytes. As the murine MC38 model behaved like the human HCT116 model (data not shown) and represents a well-established mouse model for checkpoint therapy,[46] we investigated next the effect of treatments in fully immunocompetent mice. Studies were performed with both MC38[wt] as well as MC38 cells without Mct4 (MC38[Mct4−/−]) to investigate therapy-related stromal effects. Oral administration of MCT inhibitors achieved sufficiently high serum levels in mice (MCT4i: 7.18 µM±3.07µM; MCT1i: 9.73±2.37µM; mean±SD). MC38[wt] showed limited expression of Mct1, but high expression of Mct4. As for HCT116, expression of Mct4 was further increased in MC38 3D spheroids. High levels of Mct4 were also detected in MC38 tumors (figure 4A). Thus, we treated MC38[wt] tumor-bearing mice with either MCT4i or murine aPD-L1 antibodiy alone or both MCT4i and aPD-L1 antibody. Since we could not exclude an additional impact of MCT1 inhibition, we also applied the triple combination of MCT4i, MCT1i and aPD-L1 antibody (figure 4B). Toxicity, in terms of body weight loss or liver weight increase, was not observed (online supplemental figure S4A). The impact of ICB on tumor growth and survival was significantly improved by MCT4i, which had no effect when administered alone (figure 4C,D). Triple treatment with MCT1i, MCT4i and ICB was not superior to dual MCT4i and ICB treatment (figure 4C,D). To understand whether the effect of MCT4i was driven by MCT4 expression in either tumor or stroma or both, we used MC38[Mct4−/−] tumor cells for further experiments. In line with our results on HCT116 [Mct4−/−], MC38 [Mct4−/−] tumor cells were not sensitive to MCT4i inhibition but to MCT1i (online supplemental figure S4B). Therefore, we inoculated MC38[Mct4−/−] tumor cells (online supplemental figure S4B) and administered aPD-L1 and MCT4i alone and in combination. Mct4 knock-out did not affect tumor growth kinetics (figure 4E). However, in MC38[Mct4−/−], ICB alone reduced tumor growth to a level comparable to MC38[wt] tumors treated with ICB and MCT4i up to day 13 (figure 4E). This early effect on ICB treatment was transient and prolonged survival only by trend, whereas MC38[Mct4−/−] tumor-bearing animals receiving both,

aPD-L1 and MCT4i, showed significantly better survival compared with vehicle (online supplemental figure S4C). These data might indicate that initially MCT4i acts mainly on tumor cells, but thereafter it also impacts stromal cells.

Finally, we aimed to delineate whether the treatment-related delay in tumor growth and improvement in survival in MC38[wt] tumor-bearing mice was due to an improved antitumor immune response. Interestingly, spleen weights at termination were significantly increased in all groups receiving aPD-L1 antibody (online supplemental figure S4E). We analyzed tumor immune cell infiltration at a time point when treatment effects on tumor growth were already detectable, while tumor sizes did not differ yet much between the experimental groups (online supplemental figure S4F). Hence, animals were terminated after two treatment cycles, tumors dissected, and immune cell infiltration and activation analyzed (see gating strategy online supplemental figure S4D). The portion of CD3^{+} T cells was increased by ICB but significantly elevated only after combination with MCT4i (figure 4F). Among T-cell subpopulations, the percentage of CD8^{+} T cells was significantly increased (figure 4G) and a decrease in CD4^{−}CD8^{−} T cells was observed (online supplemental figure S4G). The amount of Tregs was not altered. The main difference observed in the CD11b^{+} myeloid compartment was a reduced frequency of suppressive CD11b^{+}GR1^{+} cells by the combination of MCT4i and ICB, whereas overall percentages of myeloid cells, macrophages (F4/80^{+}) or NK cells, NK (NK1.1^{+}) and NKT cells (CD3^{+} NK1.1^{+}) were not altered by either treatment (online supplemental figure S4G). As an IFNγ-driven gene signature correlates with the response to ICB in patients,[47 48] we investigated whether MCT4 blockade affected IFNγ expression in tumor infiltrating T cells. Indeed, the amount of IFNγ expressing CD8^{+} T cells was increased by the combined treatment but not the portion of CD25 expressing T cells (figure 4H,I), whereas no impact was detected on IFNγ-expressing CD4^{+} T cells, NK cells or NKT cells (online supplemental figure S4G). The observed effects were restricted to tumor infiltrating CD8^{+} lymphocytes and CD11b^{+} cells as no differences were observed in spleen, blood or the draining lymph nodes (online supplemental figure S4H).
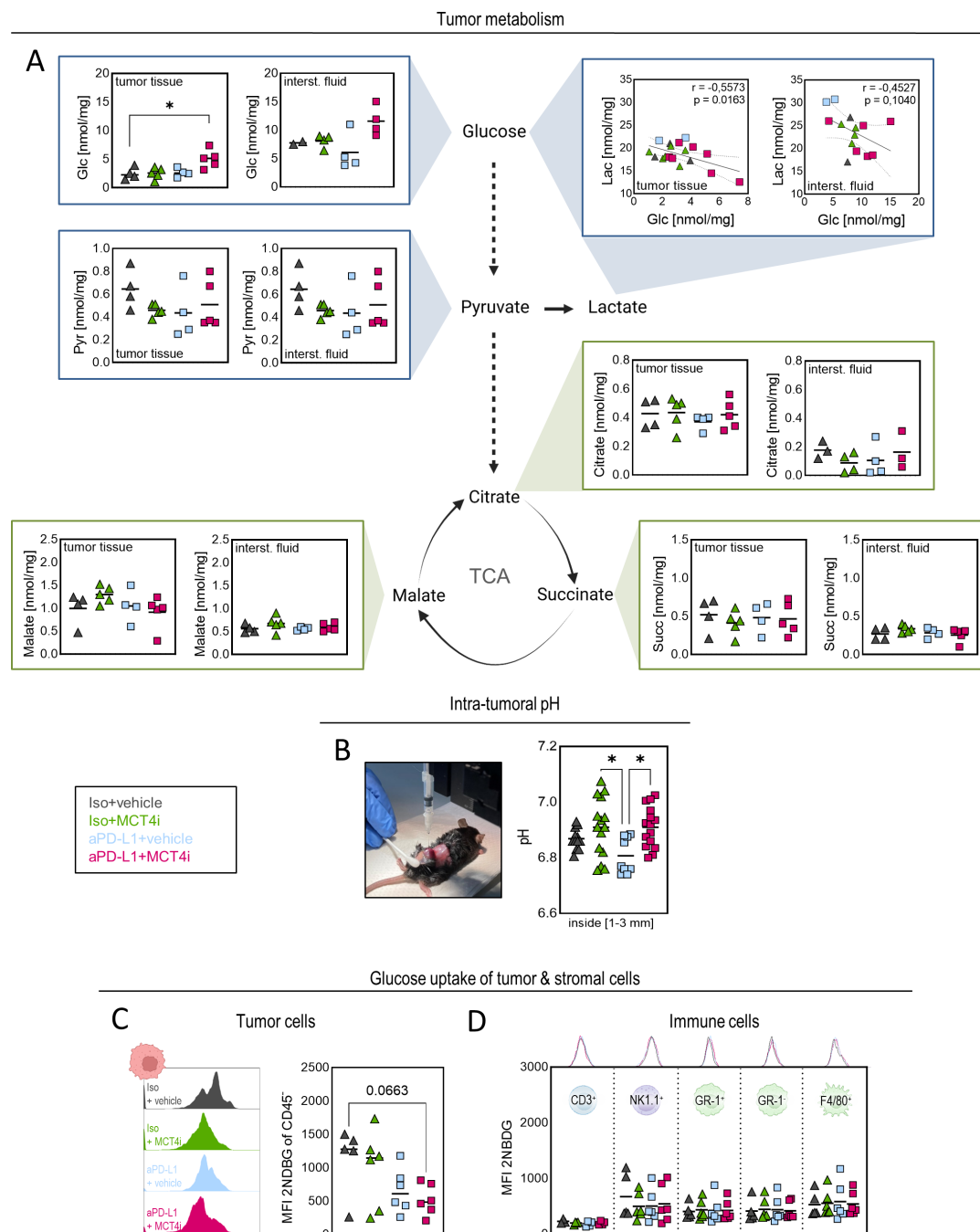
MCT4 inhibition mitigates the Warburg phenotype in vivo

As MCT4 is the dominant proton coupled lactate transporter in MC38[wt] tumor cells, its blockade should result in intracellular lactate accumulation and elevated extracellular pH. Moreover, it is known that lactate accumulation can exert a feedback inhibition on cellular glucose metabolism. Surprisingly, MCT4i treatment did not alter glucose levels neither in tumor tissue nor in interstitial fluid. However, intratumoral glucose concentrations were significantly elevated in tumors treated with MCT4i and ICB (figure 5A). Furthermore, intratumoral glucose levels inversely correlated with lactate levels in total tissue as well as in the interstitial fluid, indicating that the combined treatment had indeed reduced glucose flux
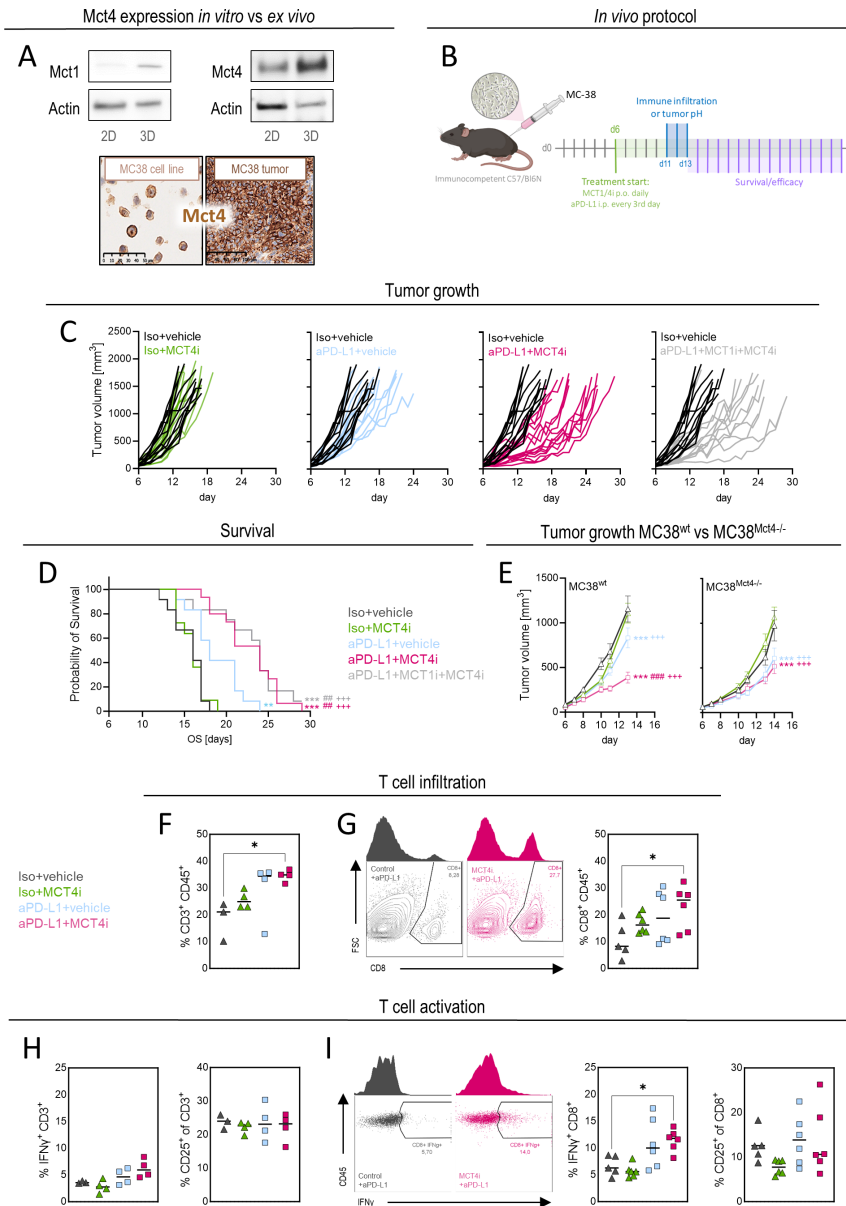
Figure 4 MCT4 blockade improves the efficacy of immune checkpoint blockade in vivo. (A) Mct1 and Mct4 expression in MC38 cells, cultured either as monolayer, spheroids or in ex vivo tumor tissue, was determined by western blot analysis (n=3) or in tumor tissue by immunohistochemistry. One representative blot out of three independent experiments is shown. (B) Protocol for in vivo experiments. 1×10^6 MC38 cells were injected subcutaneously into the flank of C57BL/6 mice. Treatment was started on day 6 after cell implantation. MCT inhibitors were administered p.o. daily (AZD3965 MCT1 inhibitor (MCT1i) 100 mg/kg body weight; MSC-4381 MCT4 inhibitor (MCT4i) 30 mg/kg body weight). Murine anti-PD-L1 antibody or respective isotype (10 mg/kg body weight) were administered i.p. every third day). For survival studies, animals were treated until the endpoint was reached. For immune infiltration and tumor pH studies, animals were treated and tumors collected on days 11–13 (two complete treatment cycles). Created with BioRender.com. (C) Individual tumor growth curves. Each line represents one mouse. (D) Survival was plotted as Kaplan-Meier estimation curves. Significance was calculated by applying the log-rank (Mantel-Cox) test with correction for multiple testing (Bonferroni correction of the p value for the number of statistical tests (n=10) performed (significant differences: *compared with vehicle, # compared with aPD-L1 antibody, + compared with to MCT4i; **p<0.01 ***p<0.001; ##p<0.01; +++p < 0.001). (E) Tumor volume of MC38^{wt} and MC38$^{Mct4-/-}$ tumors was monitored over time. Mean±SEM is shown. Significance was determined by two-way ANOVA and post hoc Bonferroni multiple comparison test (significant differences: *compared with vehicle, #compared with aPD-L1 antibody, +compared with to MCT4i; ***p<0.001; ##p<0.01; +++p < 0.001). (F–I) Gated on single, viable cells. (F) Percentage of CD3$^+$ T cells among CD45$^+$ cells determined by flow cytometry. (G) Percentage of CD8$^+$ T cells among CD45$^+$ cells determined by flow cytometry. (H) Percentage of interferon γ (IFNγ$^+$) or CD25 positive cells among CD3$^+$ T cells determined by flow cytometry. (I) Percentage of IFNγ$^+$ or CD25 positive cells among CD8$^+$ T cells determined by flow cytometry. (F–I) Representative plots and median values with single data points are shown. Significance was determined using one-way ANOVA and post hoc Bonferroni multiple comparison test (*p<0.05), unless indicated otherwise. ANOVA, analysis of variance; aPD-L1, anti-programmed cell death ligand-1; i.p., intraperitoneally; Iso, isotype; MCT, monocarboxylate transporter; p.o., orally.

Figure 5 MCT4 inhibition attenuates the Warburg phenotype of MC38 tumors. 1×10^6 MC38 cells were injected subcutaneously into the flank of C57BL/6 mice. Treatment was started on day 6 after cell implantation. MCT inhibitors were administered p.o. daily (AZD3965 MCT1 inhibitor (MCT1i) 100 mg/kg body weight; MSC-4381 MCT4 inhibitor (MCT4i) 30 mg/kg body weight). Murine anti-PD-L1 antibody or respective isotype (10 mg/kg body weight) were administered i.p. every third day, one treatment cycle consists of 2 days of MCTi alone+1 day of MCTi combined with aPD-L1 antibody. For tumor pH studies, animals were treated and tumors collected on days 11–13 (two complete treatment cycles). (A) Intratumoral concentrations of glucose (Glc), pyruvate (Pyr), citrate, succinate (Succ) and malate were determined in interstitial fluid (interst. fluid) and total tissue (snap-frozen in liquid nitrogen after extraction of interstitial fluid) by gas chromatography-mass spectrometry. Glucose plotted against lactate (Lac) concentrations in total tumor tissue and interstitial fluid. Correlation was computed using Pearson correlation test. (B) Tumor pH was measured using a microprobe pH meter at a depth of 1, 2 and 3 mm. Median values with single data points are shown. (C) Glucose uptake by viable CD45⁻ cells was determined by 2-deoxy-2-[(7-nitro-2,1,3-benzoxadiazol-4-yl)amino]-D-glucose (2NBDG) staining and analysis by flow cytometry. MFI, median fluorescence intensity. (D) 2NBDG signal in viable cell leukocyte populations (CD3⁺ T cells, NK1.1⁺ cells, Gr-1⁺ and Gr-1⁻ tumor-associated myeloid cells and F4/80⁺ macrophages). (A–D) Single data points and median values are shown. Significance was determined using one-way ANOVA and post hoc Bonferroni multiple comparison test (*p<0.05). Graphics depicting cells are created with BioRender.com. ANOVA, analysis of variance; aPD-L1, anti-programmed cell death ligand-1; i.p., intraperitoneally; Iso, isotype; MCT, monocarboxylate transporter; MCTi, MCT inhibitor; p.o., orally; TCA, tricarboxylic acid cycle.

(figure 5A). Intratumoral pH, determined at a depth of 1–3 mm, was elevated in the MCT4i treatment groups independent of ICB (figure 5B). To gain further insight on a cellular level, we measured 2-deoxy-2-[(7-nitro-2,1,3-benzoxadiazol-4-yl)amino]-D-glucose (2NBDG) uptake in CD45⁻ tumor cells and different immune cell populations. In line with increased intratumoral glucose levels, 2NBDG uptake was lower in CD45⁻ cells from MCT4i+ICB treated tumors (figure 5C). No impact was observed on T cells, NK cells, macrophages and myeloid cells regardless of GR-1 expression, indicating that tumor cells were the main therapeutic target (figure 5D). Despite its impact on glucose uptake, MCT4 inhibition did not affect the levels of pyruvate and tricarboxylic acid cycle (TCA) metabolites (figure 5A).

DISCUSSION

Over the last years, MCTs emerged as attractive targets in the context of cancer therapy. Up to now, only a limited number of studies investigated the impact of specific MCT inhibition in the context of immunotherapy.[17]

In our study, we investigated the effects of the recently described highly potent and selective carboxylic MCT4 inhibitor MSC-4381[38] and the selective MCT1 inhibitor AZD3965 in combination with ICB. In accordance with previous studies,[13 38–41] monotherapy with MCT1 or MCT4 inhibitors in 2D cultures had no effect on lactate secretion, while combined treatment diminished lactate efflux. However, in our human co-culture model of 3D colon tumor spheroids with whole blood leukocytes, which reflects more accurately the tumor microenvironment,[44] MCT4 expression was strongly elevated. In this setting, exclusive MCT4 inhibition was sufficient to reduce lactate secretion, improve T-cell function and, in combination with anti-PD-L1 treatment, foster tumor cell lysis. Similar results were obtained with an undisclosed non-carboxylic successor of MSC-4381 (data not shown). Those results could be translated to an in vivo CRC tumor model, where MCT4i and anti-PD-L1 co-administration significantly improved T-cell tumor infiltration and function and reduced the frequency of suppressive myeloid cells.

Our results are in accordance with studies showing that lactic acid contributes to immune escape and tumor progression as it severely impairs effector functions of T cells and NK cells[9 13] and fosters the differentiation and activity of tumor-promoting immune cell populations, such as Tregs[10 11 49] and myeloid cells.[7] Moreover, a highly glycolytic tumor metabolism has been linked to limited efficacy of ICB in melanoma[13 50] and renal cell carcinoma[51] and also to resistance to adoptive T-cell transfer in melanoma.[12] Therefore, restricting lactic acid secretion is a promising strategy to overcome glycolysis-related therapy resistance.

So far, multiple compounds have been described to non-specifically inhibit MCTs, such as cinnamate-based compounds,[52] syrosingopine[53] or diclofenac[13] and specific MCT1 inhibitors have been reported with clinical potential, such as AZD3965,[16] AR-C155858[54] and BAY-8002.[55] However, among specific MCT inhibitors only AZD3965 has been tested to date in a Phase I clinical trial (https://clinicaltrials.gov/ct2/show/results/NCT01791595).[56] In contrast to MCT1, which is almost ubiquitously expressed, MCT4 is predominantly found on highly glycolytic cells. This is partially explained by the fact that its expression is triggered by HIF-1α, a master regulator of the cellular response to hypoxia.[57] Based on the restricted expression, MCT4 might be a superior target, exerting less side effects compared with MCT1. However, the range of selective MCT4 inhibitors is very limited. The carboxylic compounds AZ1422,[58] VB124[59] and MSC-4381[38] represent a first generation of selective MCT4 inhibitors, while newer, non-carboxylic compounds AZD0095[42] or an undisclosed successor of MSC-4381 combine selectivity with more favorable property profiles, indicating possibilities for further improved compounds. Fang et al recently showed that VB124 can improve the response to ICB in vivo in a hepatocellular carcinoma model system by increasing CD8⁺ T-cell infiltration and function. Furthermore, they demonstrated that MCT4 knockdown reduced glycolytic activity of tumor cells and, consequently, extracellular acidification.[17] In line, MSC-4381 MCT4 inhibitor in combination with aPD-L1 increased intratumoral glucose concentrations and concomitantly, decreased glucose uptake by MC38 tumor cells. Moreover, this treatment reduced intratumoral acidification compared with anti-PD-L1 monotherapy. Our results are consistent with the observation that suppression of T-cell effector functions can be reversed in patients with acute myeloid leukemia by administration of sodium bicarbonate to buffer excess hydrogen ions.[60] However, the administration of bicarbonate could only partially mimic the effects of MCT4i administration in the HCT116 co-culture model indicating that not only the pH but also the lactate level is involved in T-cell regulation.

Nevertheless, targeting MCT4 might not only affect tumor cells. Beside tumor cells, activated T cells and tumor-infiltrating myeloid cells rely on glycolysis and contribute to lactate secretion.[61 62] Thus, MCT inhibition could impair their function. Notably, we observed improved T-cell infiltration and function in the presence of an MCT4 inhibitor in vitro and in vivo. Accordingly, we had observed previously preserved functionality of T cells, in which the MCT4 had been knocked out.[13] Apart from tumor cells and T cells, tumor-associated myeloid cells are important producers of lactate.[2] Reinfeld et al demonstrated that microbead-isolated CD11b⁺ myeloid cells from MC38 tumors showed the highest capacity for uptake of fluorodeoxyglucose.[61] Moreover, it was shown that tumor-associated macrophages expressed lactate dehydrogenase A, the myeloid-specific deletion of which supported T cell antitumor response and reduced tumor growth.[63] In line, Tan et al recently reported MCT4 expression in human and mouse bone marrow-derived macrophages.[64] Therefore, to differentiate the effect of MCT4i

in tumor versus stromal cells, we studied the impact of MCT4 inhibition in an MC38$^{Mct4-/-}$ model. In the initial phase, anti-PD-L1 treatment was not improved by MCT4 inhibition in MC38$^{Mct4-/-}$ tumors, but later survival was prolonged only by combined treatment with MCT4i and anti-PD-L1. This suggests that inhibition of MCT4 in both tumor and stromal cells is required to improve survival.

Surprisingly, additional blockade of MCT1 using specific inhibitors, counteracted the beneficial effect of MCT4 inhibition on T-cell response in co-culture with HCT116 spheroids and impaired T-cell proliferation. In line, Murray *et al* postulated that MCT1 might be important for proliferation and proposed MCT1 as target for suppression of T cells.[16] In our previously published study on the impact of diclofenac, we did not detect these adverse effects on T cells in vitro. The underlying reason could be that diclofenac blocks MCT4 with much higher potency than MCT1[13] and probably, it is less effective than a selective MCT1 inhibitor. While a negative effect was seen in vitro, we observed no undesirable in vivo effect combining MCT1 and MCT4 inhibitors compared with MCT4 monotherapy, but also no additional benefit. This suggests that MCT4 plays a more important role than MCT1 in the MC38 model. However, MCT1 inhibition might be required in MCT1-driven tumors such as 4T1, in which diclofenac as MCT1/4 dual inhibitor augmented the response to ICB.[13]

Glycolysis[2 3 9 25 65] and MCT4[5 18 26 66–68] expressions have been implicated in tumor aggressiveness and worse patient survival in various cancers. By analyzing the expression of six Warburg-related proteins, including MCT4, Offermans *et al* demonstrated that patients with CRC with Warburg-high tumors also have a worse outcome than patients with Warburg-low tumors.[25] In addition, others have found a correlation between MCT4 expression analyzed by immunohistochemistry (IHC) and survival of patients with CRC.[26 67 68] Nevertheless, when analyzing SLC16A3 encoding MCT4 in TCGA data, we found a correlation with survival only in rectal cancer, but not in colon cancer. Consistent with this, Mirnezami *et al* found higher lactate levels in rectal cancers than in colon cancers.[29] However, all studies reporting a prognostic value of MCT4 relied on IHC staining, suggesting that bulk messenger RNA expression data might sometimes fail to reflect protein expression.

Moreover, multiple studies have shown that CD8$^+$ T-cell infiltration is prognostic for overall survival in several tumor entities,[69–72] including CRC.[31 32] CRC is the second most common cause for cancer death.[23] Nevertheless, treatment strategies for CRC are limited and ICB is restricted to a small subset of 15% of tumors with MMRd/MSI.[35] Interestingly, a prognostic role of a high IFNγ signature for response to ICB has been discussed in the context of melanoma[47] and CRC.[48] Moreover, the abundance of cytotoxic T cells has been associated with response to immunotherapy in MSI CRC tumors.[36] In line, Vasaikar *et al* found a negative correlation between CD8$^+$ T cell count and increased glycolysis in MSI-high

CRC tumors,[37] suggesting that the Warburg effect limits the efficacy of ICB.[2] Our data provide the rationale that MCT4 inhibition could expand the application range and efficacy of ICB treatment for patients with CRC.

Overall, our findings demonstrate that MCT4 inhibition can reverse lactic acid-driven immunosuppression, and thereby enhance ICB response in CRC in vitro and in vivo models with predominant MCT4 expression. However, the Warburg effect represents a metabolic checkpoint across multiple cancer entities. In light of our analysis, together with the work of Bovenzi *et al*,[18] multiple solid cancers have higher MCT4 than MCT1 expression. Thus, patients with different tumor entities might benefit from combined MCT4 inhibition and ICB, as suggested by our preclinical data on CRC and the study of Fang *et al* on hepatocellular carcinoma.[17] Finally, we would like to emphasize that our human co-culture model of tumor spheroids and leukocytes reliably predicted in vivo effects. Therefore, we encourage the scientific community to use such an approach to study antitumor immune responses to complement and refine animal experiments.

METHODS

Tumor cell line culture
HCT116 tumor cell line (ATCC), MC38 tumor cell line (Scripps Research Institute) and MC38-OVA-GFP tumor cell line (provided by Ramon Arens) were cultured in RPMI1640 (Thermo Fisher Scientific) supplemented with 10% fetal calf serum (FCS, heat-inactivated, Millipore Sigma) and 2 mM L-glutamine (PAN-Biotech) in a humidified atmosphere (5% CO_2, 95% air) at 37°C in a Heraeus incubator.

Generation of HCT116 and MC38 MCT4 CRISPR knock-out clones
MC38 MCT4$^{-/-}$ cells were generated by CRISPR/Cas9 technology. HCT116$^{MCT4-/-}$ cells were generated by Horizon Discovery. For detailed information refer to online supplemental material.

Human T-cell isolation, stimulation and culture
Peripheral blood mononuclear cells were isolated by density gradient centrifugation over Ficoll/Hypaque as described[73] and either CD3$^+$ or CD8$^+$ T cells were isolated by magnetic bead separation (Miltenyi Biotec) and stimulated with anti-CD3/CD28 coated Dynabeads. For detailed information refer to online supplemental material.

Monitoring of pH and oxygen consumption in vitro
The extracellular pH and oxygen consumption of cells were monitored non-invasively over time under cell culture conditions using the PreSens technology. 0.2×10^6 tumor cells or 0.8×10^6 T cells were seeded in 1 mL in HD24 HydroDish (pH monitoring) or OD24 OxoDish (Oxygen consumption, both PreSens Precision Sensing GmbH) with pre-calibrated sensors at the bottom of each

well for non-contact reading by the SDR SensorDish Reader through the transparent material of the plate.

Determination of cell number

Cell proliferation in culture was monitored using the CASY Cell Counter system (Omni Life Science).

Determination of cytokines

Cytokine secretion was determined in 48 hours culture supernatants by commercially available enzyme-linked immunosorbent assays (R&D Systems) according to the manufacturer's protocol.

Determination of glucose uptake

Glucose concentration in culture supernatants was measured using the Glucose HK assay Kit (Sigma Aldrich). In brief, 5 μl culture supernatant were mixed with 195 μl reconstituted assay reagent in a 96-well microplate, incubated for 15 min and absorbance at 340 nm measured using a microplate reader. Glucose levels were quantified by means of a standard curve. To calculate glucose uptake, measured glucose concentration in supernatants was subtracted from glucose concentration in medium.

Quantification of lactate secretion

Tumor cells ($2.5 \times 10^4 / 200 \mu L$) or T cells ($0.1 \times 10^6 / 200 \mu L$) were seeded into flat-bottom and round bottom 96-well plates for 24 hours or 48 hours, respectively. Lactate concentrations in cell culture supernatants were determined enzymatically by the Department of Clinical Chemistry at the University Hospital of Regensburg, Germany.

Co-culture of HCT116 tumor spheroids and human immune cells

HCT116 spheroids were grown from 2D cultures. On day 4 after seeding, spheroids were treated with 0.1 μM MCT inhibitors. On day 12, MNCs and peripheral mononuclear cells (PMNs) were isolated from peripheral blood of healthy donors and unstimulated 0.1×10^6 immune cells added to the spheroids. MNCs of the same donor were stimulated with anti-CD3/CD28 coated Dynabeads and after 24 hours 0.1×10^6 MNCs, mainly T cells, were added along with IL-2, aPD-L1 or a mutant isotype control, and MCT inhibitors were replenished. After further 24 hours of co-culture, spheroids were collected and prepared for live-cell imaging or flow cytometry. For detailed information refer to online supplemental material.

Co-culture of MC38-OVA-GFP tumor spheroids and murine immune cells

MC38-OVA-GFP spheroids were grown from 2D cultures. After 3 days, spheroids were treated with MCT inhibitors and incubated for seven further days. Co-culture was started on day 10. Immune cells were isolated from spleens of 16–20 weeks old OT-I mice, B cells were removed by magnetic separation, and unstimulated splenocytes added. In addition, antigen-specific T cells were stimulated by incubation with SIINFEKL-peptide for 24 hours. Stimulated T cells were added along with IL-2,

IL-15, aPD-L1 or respective isotype control, and MCT inhibitors were replenished. Spheroids were cultivated with immune cells for an additional 48 hours before Live-Cell Imaging was performed. For detailed information refer to online supplemental material.

Real-time live cell imaging

Spheroid lysis was detected using the real-time live cell imaging system IncuCyte ZOOM (Sartorius). For detailed information refer to online supplemental material.

Mice and in vivo experiments

Animal experiments on tumors were performed according to the regulations of the local government of Würzburg, Germany, and permission was obtained from the Government of Unterfranken, Germany.

To generate MC38 tumors in mice, 1×10^6 MC38^{wt} or MC38$^{MCT4-/-}$ tumor cells were injected in 50 μl RPMI 1640 medium subcutaneously in the dorsal region. MSC-4381 MCT4i was administered at 30 mg/kg body weight, AZD3965 MCT1i was administered at 100 mg/kg body weight, both at a volume of 10 mL/kg body weight. MCT inhibitors were given per os (p.o.) daily, starting on day 6 after tumor inoculation. Murine Anti-PD-L1 (Bio X Cell) and rat IgG2b isotype (Iso) (Bio X Cell) antibodies were administered intraperitoneal at a concentration of 10 mg/kg every third day, starting on day 6 after tumor inoculation. All treatments were continued for the entire duration of the study. Tumor volume was determined by using the tumor length (l) and width (w) measurements. At indicated time points blood, spleens, lymph nodes and tumors were harvested for analysis. For detailed information refer to online supplemental material.

Determination of intratumoral pH

Tumor pH was determined in size matched tumors by a microfiber optic pH meter with needle-type housed pH microsensors (20/0.4) using a manual micromanipulator (PreSens Precision Sensing GmbH). MCT inhibitors were administered 2 hour prior to pH measurement. Microsensors were calibrated for at least 30 min, tumors were dissected and pH microsensor was inserted 1–3 mm into the tumor and pH was reported between 1–3 min with the software pH1-View.

Flow cytometry

Single cell suspensions were stained for flow cytometry. Apoptosis was determined by Annexin-V/ 7-AAD staining. Glucose uptake was assessed by staining with 2-(N-(7-Nitrobenz-2-Oxa-1,3-Diazol-4-yl)Amino)−2-Deoxyglucose (2-NBDG; Thermo Fisher Scientific). For live-dead discrimination, cells were stained with Zombie-NIR (BioLegend). Surface staining was performed in phosphate buffered saline (PBS) with 2% FCS for 20 min at 4°C. For intracellular detection of cytokines, cells were incubated with monensin prior to staining, surface staining was performed and intracellular staining was performed after fixation/permeabilization using the eBioscience Foxp3/Transcription Factor Staining Buffer

(eBioscience). Stainings were performed in PBS+2% FCS for 20 min at 4°C. All antibodies were purchased from BD Biosciences or BioLegend. For detailed information refer to online supplemental material.

Determination of intermediates of glycolysis and TCA cycle in tumor tissue and interstitial fluid

Interstitial fluid was extracted from tumor tissue according to a protocol by Wiig et al.[74] TCA intermediates in tumor tissue and interstitial fluid were assessed by gas chromatography coupled mass spectrometry (GC-MS) after methanol precipitation. For detailed information refer to online supplemental material.

Western blot analysis

Protein expression was analyzed by western blot. For detailed information refer to online supplemental material.

Immunohistochemistry

IHC was performed on formaldehyde-fixed paraffin embedded tissue or tissue/cell microarrays mounted on positively charged SuperFrostPlus slides. Horseradish peroxidase conjugated polymers were used to visualize staining. Sections were counterstained with hematoxylin. Immunohistochemical stains were scanned with the NanoZoomer (Hamamatsu). Microscopic evaluation was done using the Polyvar 2 microscope (Leica). For detailed information refer to online supplemental material.

Chemicals

MCT inhibitors were first dissolved in dimethyl sulfoxide (DMSO) at a concentration of 10 mM and further diluted in RPMI1640 to stock concentration of 100 µM (final concentration 0.1 µM or 2 µM were used as indicated). Human anti-PD-L1 and mutated isotype control were provided by the Healthcare business of Merck KGaA, Darmstadt, Germany (CrossRef Funder ID: 10.13039/100009945) or the University Hospital Regensburg. Murine anti-PD-L1 and rat IgG2b isotype (Iso) were obtained from Bio X Cell. Lactic acid and cell-culture grade HCl were purchased by Sigma Aldrich, sodium bicarbonate was obtained from Roth Chemicals.

Database analyses

Transcriptome data from 430 colorectal, 326 colon cancer and 186 rectal cancer samples were obtained from TCGA database using the UCSC Xena platform.[75] Expression is depicted as log2(fpkm-uq+1) values. Log-rank (Mantel-Cox) test was used to calculate differences in OS when comparing the upper and the lower quartile of samples.

Kaplan-Meier estimation curves for OS of individual patients with CRC from a second cohort were generated with the microarray analysis and visualization platform R2 (http://r2.amc.nl) by using the "R2: Tumor Colon (after surgery) - Beissbarth - 363 - custom - 4hm44k" data set. For determination of high and low expression of SLC16A3 the cut-off modus "scan" divided the patients into two groups. The raw p value significance was calculated for every graph using the web database.

Statistical analysis

Statistical parameters including the exact value of n, the definition of the center, dispersion, and precision and statistical significance are reported in the figures and the figure legends. Statistical analysis was performed with the GraphPad Prism software (versions 9 and 10). Data were judged to be statistically significant when $p < 0.05$. For comparison of more than two groups or time points, one-way or two-way analysis of variance with post hoc Bonferroni's or Dunnett multiple comparison test was used, whereas paired or unpaired/two-tailed Mann-Whitney U or Wilcoxon's matched pair signed rank test were applied to the comparison of two groups. For Kaplan-Meier curves, significance was calculated by applying the log-rank (Mantel-Cox) test with correction for multiple testing (Bonferroni correction of the p value for the number of statistical tests (n=10) was performed). Asterisks in figures denote statistical significance (*$p < 0.05$, **$p < 0.01$, ***$p < 0.001$).

Author affiliations

[1]Department of Internal Medicine III, University Hospital Regensburg, Regensburg, Germany
[2]Department of Otorhinolaryngology, University Hospital Regensburg, Regensburg, Germany
[3]Leibniz Institute for Immunotherapy, Regensburg, Germany
[4]Merck Healthcare KGaA, Darmstadt, Germany
[5]EMD Serono Research and Development Institute, Inc, Billerica, Massachusetts, USA, an affiliate of Merck KGaA
[6]Department of Surgery, University Hospital Regensburg, Regensburg, Germany
[7]Department of Gynecology and Obstetrics, University Hospital Regensburg, Regensburg, Germany
[8]Institute of Functional Genomics, University of Regensburg, Regensburg, Germany

ORCID iDs
Nathalie Babl http://orcid.org/0000-0002-5584-322X
Peter Siska http://orcid.org/0000-0002-1521-6213

REFERENCES

1 Hanahan D, Weinberg RA. Hallmarks of cancer: the next generation. *Cell* 2011;144:646–74.
2 Siska PJ, Singer K, Evert K, *et al*. The immunological Warburg effect: can a metabolic-tumor-Stroma score (Mets) guide cancer Immunotherapy. *Immunol Rev* 2020;295:187–202.
3 Walenta S, Wetterling M, Lehrke M, *et al*. High lactate levels predict likelihood of metastases, tumor recurrence, and restricted patient survival in human Cervical cancers. *Cancer Res* 2000;60:916–21.
4 Pinheiro C, Longatto-Filho A, Azevedo-Silva J, *et al*. Role of Monocarboxylate transporters in human cancers: state of the art. *J Bioenerg Biomembr* 2012;44:127–39.
5 Choi J-W, Kim Y, Lee J-H, *et al*. Prognostic significance of lactate/proton Symporters Mct1, Mct4, and their chaperone Cd147 expressions in urothelial carcinoma of the bladder. *Urology* 2014;84.
6 Noy R, Pollard JW. Tumor-associated Macrophages: from mechanisms to therapy. *Immunity* 2014;41:49–61.
7 Colegio OR, Chu N-Q, Szabo AL, *et al*. Functional polarization of tumour-associated Macrophages by tumour-derived lactic acid. *Nature* 2014;513:559–63.
8 Mendler AN, Hu B, Prinz PU, *et al*. Tumor lactic acidosis suppresses CTL function by inhibition of P38 and JNK/C-Jun activation. *Int J Cancer* 2012;131:633–40.
9 Brand A, Singer K, Koehl GE, *et al*. LDHA-associated lactic acid production blunts tumor Immunosurveillance by T and NK cells. *Cell Metab* 2016;24:657–71.
10 Angelin A, Gil-de-Gómez L, Dahiya S, *et al*. Foxp3 Reprograms T cell metabolism to function in low-glucose, high-lactate environments. *Cell Metab* 2017;25:1282–93.
11 Watson MJ, Vignali PDA, Mullett SJ, *et al*. Metabolic support of tumour-infiltrating regulatory T cells by lactic acid. *Nature* 2021;591:645–51.
12 Cascone T, McKenzie JA, Mbofung RM, *et al*. Increased tumor Glycolysis characterizes immune resistance to adoptive T cell therapy. *Cell Metab* 2018;27:977–87.
13 Renner K, Bruss C, Schnell A, *et al*. Restricting Glycolysis preserves T cell Effector functions and augments Checkpoint therapy. *Cell Rep* 2019;29:135–50.
14 Reckzeh ES, Waldmann H. Small-molecule inhibition of glucose transporters GLUT-1-4. *Chembiochem* 2020;21:45–52.
15 Granchi C, Paterni I, Rani R, *et al*. Small-molecule inhibitors of human Ldh5. *Future Med Chem* 2013;5:1967–91.
16 Murray CM, Hutchinson R, Bantick JR, *et al*. Monocarboxylate transporter Mct1 is a target for immunosuppression. *Nat Chem Biol* 2005;1:371–6.
17 Fang Y, Liu W, Tang Z, *et al*. Monocarboxylate transporter 4 inhibition potentiates hepatocellular carcinoma Immunotherapy through enhancing T cell infiltration and immune attack. *Hepatology* 2023;77:109–23.
18 Bovenzi CD, Hamilton J, Tassone P, *et al*. Prognostic indications of elevated Mct4 and Cd147 across cancer types: A meta-analysis. *Biomed Res Int* 2015;2015:242437.
19 Baek G, Tse YF, Hu Z, *et al*. Mct4 defines a Glycolytic subtype of Pancreatic cancer with poor prognosis and unique metabolic dependencies. *Cell Rep* 2014;9:2233–49.
20 Baenke F, Dubuis S, Brault C, *et al*. Functional screening identifies Mct4 as a key regulator of breast cancer cell metabolism and survival. *J Pathol* 2015;237:152–65.
21 Pinheiro C, Longatto-Filho A, Scapulatempo C, *et al*. Increased expression of Monocarboxylate transporters 1, 2, and 4 in colorectal Carcinomas. *Virchows Arch* 2008;452:139–46.
22 Martins SF, Amorim R, Viana-Pereira M, *et al*. Significance of Glycolytic metabolism-related protein expression in colorectal cancer, lymph node and hepatic metastasis. *BMC Cancer* 2016;16:535.
23 Sung H, Ferlay J, Siegel RL, *et al*. Global cancer Statistics 2020: GLOBOCAN estimates of incidence and mortality worldwide for 36 cancers in 185 countries. *CA Cancer J Clin* 2021;71:209–49.
24 Javaeed A, Ghauri SK. Mct4 has a potential to be used as a Prognostic biomarker - a systematic review and meta-analysis. *Oncol Rev* 2019;13:403.
25 Offermans K, Jenniskens JC, Simons CC, *et al*. Expression of proteins associated with the Warburg-effect and survival in colorectal cancer. *J Pathol Clin Res* 2022;8:169–80.
26 Nakayama Y, Torigoe T, Inoue Y, *et al*. Prognostic significance of Monocarboxylate transporter 4 expression in patients with colorectal cancer. *Exp Ther Med* 2012;3:25–30.
27 Dong S, Liang S, Cheng Z, *et al*. ROS/Pi3K/AKT and WNT/B-Catenin Signalings activate HIF-1A-induced metabolic Reprogramming to impart 5-fluorouracil resistance in colorectal cancer. *J Exp Clin Cancer Res* 2022;41:15.
28 Jiménez B, Mirnezami R, Kinross J, *et al*. "1H HR-MAS NMR spectroscopy of tumor-induced local metabolic "field-effects" enables colorectal cancer staging and prognostication". *J Proteome Res* 2013;12:959–68.
29 Mirnezami R, Jiménez B, Li JV, *et al*. Rapid diagnosis and staging of colorectal cancer via high-resolution magic angle spinning nuclear magnetic resonance (HR-MAS NMR) spectroscopy of intact tissue biopsies. *Ann Surg* 2014;259:1138–49.
30 Liu Z, Liu Z, Zhou X, *et al*. A Glycolysis-related two-gene risk model that can effectively predict the prognosis of patients with Rectal cancer. *Hum Genomics* 2022;16:5.
31 Mlecnik B, Bindea G, Angell HK, *et al*. Integrative analyses of colorectal cancer show Immunoscore is a stronger Predictor of patient survival than Microsatellite instability. *Immunity* 2016;44:698–711.
32 Galon J, Costes A, Sanchez-Cabo F, *et al*. Type, density, and location of immune cells within human colorectal tumors predict clinical outcome. *Science* 2006;313:1960–4.
33 Anitei M-G, Zeitoun G, Mlecnik B, *et al*. Prognostic and predictive values of the Immunoscore in patients with Rectal cancer. *Clin Cancer Res* 2014;20:1891–9.
34 Angell HK, Bruni D, Barrett JC, *et al*. The Immunoscore: colon cancer and beyond. *Clin Cancer Res* 2020;26:332–9.
35 Ganesh K, Stadler ZK, Cercek A, *et al*. Immunotherapy in colorectal cancer: rationale, challenges and potential. *Nat Rev Gastroenterol Hepatol* 2019;16:361–75.
36 Dolcetti R, Viel A, Doglioni C, *et al*. High prevalence of activated intraepithelial cytotoxic T lymphocytes and increased neoplastic cell apoptosis in colorectal Carcinomas with Microsatellite instability. *The American Journal of Pathology* 1999;154:1805–13.
37 Vasaikar S, Huang C, Wang X, *et al*. Proteogenomic analysis of human colon cancer reveals new therapeutic opportunities. *Cell* 2019;177:1035–1049.
38 Heinrich T, Sala-Hojman A, Ferretti R, *et al*. Discovery of 5-{2-5-Chloro-2-(5-Ethoxyquinoline-8-Sulfonamido)Phenylethynyl}-4-Methoxypyridine-2-Carboxylic acid, a highly selective in vivo useable chemical probe to dissect Mct4 biology. *J Med Chem* 2021;64:11904–33.
39 Polański R, Hodgkinson CL, Fusi A, *et al*. Activity of the Monocarboxylate transporter 1 inhibitor Azd3965 in small cell lung cancer. *Clin Cancer Res* 2014;20:926–37.
40 Doherty JR, Yang C, Scott KEN, *et al*. Blocking lactate export by inhibiting the Myc target Mct1 Disables Glycolysis and glutathione synthesis. *Cancer Res* 2014;74:908–20.
41 Marchiq I, Le Floch R, Roux D, *et al*. Genetic disruption of lactate/H+ Symporters (Mcts) and their subunit Cd147/BASIGIN sensitizes Glycolytic tumor cells to Phenformin. *Cancer Res* 2015;75:171–80.

42 Goldberg FW, Kettle JG, Lamont GM, *et al*. Discovery of clinical candidate Azd0095, a selective inhibitor of Monocarboxylate transporter 4 (Mct4) for oncology. *J Med Chem* 2023;66:384–97.

43 Roy M, Finley SD. Metabolic Reprogramming Dynamics in tumor Spheroids: insights from a Multicellular, Multiscale model. *PLoS Comput Biol* 2019;15:e1007053.

44 Tidwell TR, Røsland GV, Tronstad KJ, *et al*. Metabolic flux analysis of 3d Spheroids reveals significant differences in glucose metabolism from matched 2d cultures of colorectal cancer and Pancreatic Ductal adenocarcinoma cell lines. *Cancer Metab* 2022;10:9.

45 Macintyre AN, Gerriets VA, Nichols AG, *et al*. The glucose transporter Glut1 is selectively essential for Cd4 T cell activation and Effector function. *Cell Metab* 2014;20:61–72.

46 Selby MJ, Engelhardt JJ, Johnston RJ, *et al*. Preclinical development of Ipilimumab and Nivolumab combination Immunotherapy: Mouse tumor models. *PLOS ONE* 2016.

47 Rozeman EA, Hoefsmit EP, Reijers ILM, *et al*. Survival and biomarker analyses from the Opacin-Neo and Opacin Neoadjuvant Immunotherapy trials in stage III Melanoma. *Nat Med* 2021;27:256–63.

48 Du W, Frankel TL, Green M, *et al*. IFNγ signaling integrity in colorectal cancer immunity and Immunotherapy. *Cell Mol Immunol* 2022;19:23–32.

49 Kumagai S, Koyama S, Itahashi K, *et al*. Lactic acid promotes PD-1 expression in regulatory T cells in highly Glycolytic tumor Microenvironments. *Cancer Cell* 2022;40:201–18.

50 Daneshmandi S, Wegiel B, Seth P. Blockade of lactate dehydrogenase-A (LDH-A) improves efficacy of anti-programmed cell Death-1 (PD-1) therapy in Melanoma. *Cancers (Basel)* 2019;11:450.

51 Ascierto ML, McMiller TL, Berger AE, *et al*. The Intratumoral balance between metabolic and immunologic gene expression is associated with anti-PD-1 response in patients with renal cell carcinoma. *Cancer Immunol Res* 2016;4:726–33.

52 Jonnalagadda S, Jonnalagadda SK, Ronayne CT, *et al*. Novel N,N-Dialkyl Cyanocinnamic acids as Monocarboxylate transporter 1 and 4 inhibitors. *Oncotarget* 2019;10:2355–68.

53 Benjamin D, Robay D, Hindupur SK, *et al*. Dual inhibition of the lactate transporters Mct1 and Mct4 is synthetic lethal with metformin due to NAD+ depletion in cancer cells. *Cell Rep* 2018;25:3047–58.

54 Puri S, Juvale K. Monocarboxylate transporter 1 and 4 inhibitors as potential Therapeutics for treating solid tumours: A review with structure-activity relationship insights. *Eur J Med Chem* 2020;199:112393.

55 Quanz M, Bender E, Kopitz C, *et al*. Preclinical efficacy of the novel Monocarboxylate transporter 1 inhibitor BAY-8002 and associated markers of resistance. *Mol Cancer Ther* 2018;17:2285–96.

56 Halford S, Veal GJ, Wedge SR, *et al*. A phase I dose-escalation study of AZD3965, an oral monocarboxylate transporter 1 inhibitor, in patients with advanced cancer. *Clinical Cancer Research* 2023;29:1429–39.

57 Ullah MS, Davies AJ, Halestrap AP. The plasma membrane lactate transporter Mct4, but not Mct1, is up-regulated by hypoxia through a HIF-1Alpha-dependent mechanism. *J Biol Chem* 2006;281:9030–7.

58 Critchlow SE. *New Developments in Targeting Lactate Transporters*. AACR: Chicago, 2018.

59 Cluntun AA, Badolia R, Lettlova S, *et al*. The pyruvate-lactate axis modulates cardiac hypertrophy and heart failure. *Cell Metab* 2021;33:629–48.

60 Uhl FM, Chen S, O'Sullivan D, *et al*. Metabolic Reprogramming of donor T cells enhances graft-versus-leukemia effects in mice and humans. *Sci Transl Med* 2020;12:eabb8969.

61 Reinfeld BI, Madden MZ, Wolf MM, *et al*. Cell-programmed nutrient partitioning in the tumour Microenvironment. *Nature* 2021;593:282–8.

62 Geltink RIK, Kyle RL, Pearce EL. Unraveling the complex interplay between T cell metabolism and function. *Annu Rev Immunol* 2018;36:461–88.

63 Seth P, Csizmadia E, Hedblom A, *et al*. Deletion of lactate dehydrogenase-A in myeloid cells triggers antitumor immunity. *Cancer Res* 2017;77:3632–43.

64 Tan Z, Xie N, Banerjee S, *et al*. The Monocarboxylate transporter 4 is required for Glycolytic Reprogramming and inflammatory response in Macrophages. *J Biol Chem* 2015;290:46–55.

65 Ottensmeier CH, Perry KL, Harden EL, *et al*. Upregulated glucose metabolism correlates inversely with Cd8+ T-cell infiltration and survival in squamous cell carcinoma. *Cancer Res* 2016;76:4136–48.

66 Pinheiro C, Miranda-Gonçalves V, Longatto-Filho A, *et al*. The metabolic Microenvironment of Melanomas: Prognostic value of Mct1 and Mct4. *Cell Cycle* 2016;15:1462–70.

67 Petrides C, Neofytou K, Agrogiannis G, *et al*. Monocarboxylate transporter 4 as a Prognostic biomarker in patients with colorectal cancer and liver metastases. *International Journal of Surgery Open* 2016;5:37–43.

68 Abe Y, Nakayama Y, Katsuki T, *et al*. The Prognostic significance of the expression of Monocarboxylate transporter 4 in patients with Right- or left-sided colorectal cancer. *Asia Pac J Clin Oncol* 2019;15:e49–55.

69 Mahmoud SMA, Paish EC, Powe DG, *et al*. Tumor-infiltrating Cd8+ lymphocytes predict clinical outcome in breast cancer. *J Clin Oncol* 2011;29:1949–55.

70 Yang I, Tihan T, Han SJ, *et al*. Cd8+ T-cell infiltrate in newly diagnosed glioblastoma is associated with long-term survival. *J Clin Neurosci* 2010;17:1381–5.

71 Hu W-H, Miyai K, Cajas-Monson LC, *et al*. Tumor-infiltrating Cd8(+) T lymphocytes associated with clinical outcome in Anal squamous cell carcinoma. *J Surg Oncol* 2015;112:421–6.

72 Zhuang X, Xia X, Wang C, *et al*. A high number of Cd8+ T cells infiltrated in NSCLC tissues is associated with a favorable prognosis. *Appl Immunohistochem Mol Morphol* 2010;18:24–8.

73 Andreesen R, Scheibenbogen C, Brugger W, *et al*. Adoptive transfer of tumor cytotoxic Macrophages generated in vitro from circulating blood monocytes: a new approach to cancer Immunotherapy. *Cancer Res* 1990;50:7450–6.

74 Wiig H, Aukland K, Tenstad O. Isolation of interstitial fluid from rat Mammary tumors by a centrifugation method. *Am J Physiol Heart Circ Physiol* 2003;284:H416–24.

75 Goldman MJ, Craft B, Hastie M, *et al*. Visualizing and interpreting cancer Genomics data via the Xena platform. *Nat Biotechnol* 2020;38:675–8.